UNIVERSITY OF AMSTERDAM

UvA-DARE (Digital Academic Repository)

Fast-time Variations of Supernova Neutrino Fluxes and Detection Perspectives

Tamborra, I.; Hanke, F.; Müller, B.; Janka, H.T.; Raffelt, G.G.

DOI
10.1016/j.phpro.2014.12.076

Publication date
2015

Document Version
Final published version

Published in
Physics Procedia

License
CC BY-NC-ND

Link to publication

Citation for published version (APA):
Tamborra, I., Hanke, F., Müller, B., Janka, H. T., & Raffelt, G. G. (2015). Fast-time Variations of Supernova Neutrino Fluxes and Detection Perspectives. *Physics Procedia*, *61*, 359-365. https://doi.org/10.1016/j.phpro.2014.12.076

General rights
It is not permitted to download or to forward/distribute the text or part of it without the consent of the author(s) and/or copyright holder(s), other than for strictly personal, individual use, unless the work is under an open content license (like Creative Commons).

Disclaimer/Complaints regulations
If you believe that digital publication of certain material infringes any of your rights or (privacy) interests, please let the Library know, stating your reasons. In case of a legitimate complaint, the Library will make the material inaccessible and/or remove it from the website. Please Ask the Library: https://uba.uva.nl/en/contact, or a letter to: Library of the University of Amsterdam, Secretariat, Singel 425, 1012 WP Amsterdam, The Netherlands. You will be contacted as soon as possible.

UvA-DARE is a service provided by the library of the University of Amsterdam (https://dare.uva.nl)

Download date:09 Mar 2023

Available online at www.sciencedirect.com

ScienceDirect

Physics Procedia 61 (2015) 359 – 365

Physics Procedia

Fast-time variations of supernova neutrino fluxes and detection perspectives

I. Tamborra[a,1,*], F. Hanke[b], B. Müller[b,2], H.-T. Janka[b], G.G. Raffelt[a]

[a]*Max-Planck-Institut für Physik (Werner-Heisenberg-Institut), Föhringer Ring 6, 80805 München, Germany*
[b]*Max-Planck-Institut für Astrophysik, Karl-Schwarzschild-Str. 1, 85748 Garching, Germany*

Abstract

In the delayed explosion scenario of a core-collapse supernova, the accretion phase shows pronounced convective overturns and a low-multipole hydrodynamic instability, the so-called standing accretion shock instability (SASI). Neutrino signal variations from the first full-scale three-dimensional core-collapse supernova simulations with sophisticated neutrino transport are presented as well as their detection perspectives in IceCube and Hyper-Kamiokande.

© 2015 The Authors. Published by Elsevier B.V. This is an open access article under the CC BY-NC-ND license (http://creativecommons.org/licenses/by-nc-nd/3.0/).

Selection and peer review is the responsibility of the Conference lead organizers, Frank Avignone, University of South Carolina, and Wick Haxton, University of California, Berkeley, and Lawrence Berkeley Laboratory

Keywords: neutrinos, supernova, hydrodynamical instabilities

1. Introduction

Bethe and Wilson's delayed neutrino-driven explosion mechanism [1] remains the standard core-collapse supernova (SN) paradigm [2]. At core bounce a shock wave forms, it looses all its energy dissociating atoms within the iron shell and is then revived by neutrino heating after $\mathcal{O}(10^2)$ ms. During the accretion phase, large-scale convective overturn develops in the neutrino-heated postshock layer [3] and the standing accretion shock instability (SASI) can arise, involving sloshing motions of the shock front [4, 5] as well as spiral modes [6, 7, 8, 9, 10]. The next galactic SN may reveal these effects in gravitational waves [11, 12] as well as in neutrinos [13, 14].

Up to now, SN investigations of convection and SASI were based on axisymmetric simulations where sloshing motions are constrained to the symmetry axis. Several recent 3D models found SASI sloshing motions with considerably reduced amplitudes or no clear SASI signature at all. Convection was concluded to dominate post-shock turbulence and SASI to be a minor feature of SN dynamics. However, SASI development may depend on progenitor properties and the exact behavior of the stalled shock (which requires reliable neutrino transport) and self-consistent, 2D simulations with sophisticated neutrino transport suggest

*Corresponding author

Email addresses: i.tamborra@uva.nl (I. Tamborra), fhanke@mpa-garching.mpg.de (F. Hanke), bernhard.mueller@monash.edu (B. Müller), thj@mpa-garching.mpg.de (H.-T. Janka), raffelt@mpp.mpg.de (G.G. Raffelt)

[1]Present address: GRAPPA Institute, University of Amsterdam, Science Park 904, 1090 GL Amsterdam, The Netherlands.

[2]Present address: Monash Center for Astrophysics, School of Mathematical Sciences, Building 28, Monash University, Victoria 3800, Australia

1875-3892 © 2015 The Authors. Published by Elsevier B.V. This is an open access article under the CC BY-NC-ND license (http://creativecommons.org/licenses/by-nc-nd/3.0/).

Selection and peer review is the responsibility of the Conference lead organizers, Frank Avignone, University of South Carolina, and Wick Haxton, University of California, Berkeley, and Lawrence Berkeley Laboratory

doi:10.1016/j.phpro.2014.12.076

that SASI remains possible for small shock stagnation radii [15]. The first 3D simulation with detailed neutrino transport (a 27 $M_\odot$ SN progenitor) shows indeed violent SASI activity [10].

The SASI activity strongly modulates the neutrino emission. The detection of such fast time variations of the neutrino signal will offer a unique chance to probe stellar core collapse [13, 14]. IceCube [16] is among the most promising facilities for this task, detecting a large number of Cherenkov photons triggered by neutrinos. Moreover, Super-Kamiokande (Super-K) [17], or the next-generation Hyper-Kamiokande (Hyper-K) [18] will monitor the neutrino signal without background and provide event-by-event energy information.

We here discuss the detection opportunities for a SASI-modulated SN neutrino signal based on the world-wide first 3D simulations with detailed neutrino transport of three SN progenitors with 27 $M_\odot$, 20 $M_\odot$, and 11.2 $M_\odot$.

2. Numerical supernova models

We use solar metallicity progenitors for which the evolution until the onset of iron-core collapse has been reported in [19] for the 11.2 and 27 $M_\odot$ stars and in [20] for the 20 $M_\odot$ star. The 3D modeling uses the Prometheus-Vertex hydrodynamics code, including state-of-the-art neutrino interaction rates [21] and relativistic gravity and redshift corrections [22, 23].

The adopted description assumes the neutrino momentum distribution to be axisymmetric around the radial direction, implying that the neutrino fluxes are radial. The detectable energy-dependent neutrino emission from the hemisphere facing an observer is therefore determined with a post-processing procedure that includes projection and limb-darkening effects [24].

3. Detection perspectives: 27 $M_\odot$ supernova model

In the largest operating detectors, IceCube and Super-K, neutrinos are mainly detected by inverse beta decay, $\bar{\nu}_e + p \rightarrow n + e^+$. We represent the neutrino energy spectra in the form of Gamma distributions [25, 26] and estimate the neutrino signal as described in [27], assuming an overall background rate of $R_{\rm bkgd} = 1.48 \times 10^3$ ms^{-1} (comparable to the signal rate for a SN at 10 kpc).

IceCube will register $O(10^6)$ events above background for a SN at 10 kpc, to be compared with around 10^4 events for Super-K (fiducial mass 32 kton), i.e., IceCube has superior statistics. While the future Hyper-K will have a fiducial mass of 740 kton, providing a background-free signal of roughly 1/3 the IceCube rate. Moreover Hyper-K will provide event-by-event energy information (which we do not use here).

To get a first impression of the neutrino signal modulation we consider the 27 $M_\odot$ model [10]. Figure 1 shows the expected rate in IceCube and Hyper-K. This model shows clear SASI activity at 120–260 ms. At ~220 ms a SASI spiral mode sets in and remains confined to an almost stable plane not aligned with the polar grid of the simulation. The first SASI episode ends abruptly with the accretion of the Si/SiO interface, followed by large-scale convection with much smaller and less periodic signal modulations. After about 410 ms, SASI activity begins again until the end of our simulation. In the top panel, we select an observer located in the SASI plane in a favorable direction and show the expected IceCube signal. While the second panel of Fig. 1 is for a direction orthogonal to the plane of the first SASI episode (i.e., the signal modulation is smaller than before).

Neutrinos change their flavor as they propagate from the SN core to the detector. Other than the Mikheev-Smirnov-Wolfenstein (MSW) neutrino flavor conversions, neutrino-neutrino interactions occur while neutrinos propagate through the SN envelope. However, since we still miss a detailed picture of the impact of neutrino-neutrino interactions on the SN neutrino signal due to the non-linear nature of the problem, we choose to show the two extreme scenarios in Fig. 1. One case assumes the signal caused by unoscillated $\bar{\nu}_e$ (i.e., ignoring flavor conversions), while the other case assumes complete flavor conversion so that the signal is caused by $\bar{\nu}_x$ (with $\bar{\nu}_x$ a combination of $\bar{\nu}_\mu$ and $\bar{\nu}_\tau$). Note as both cases reveal large signal modulations with a clear periodicity and, therefore, assuming that the observed signal will be anything in between these two extreme cases, SASI modulations will be clearly detectable.

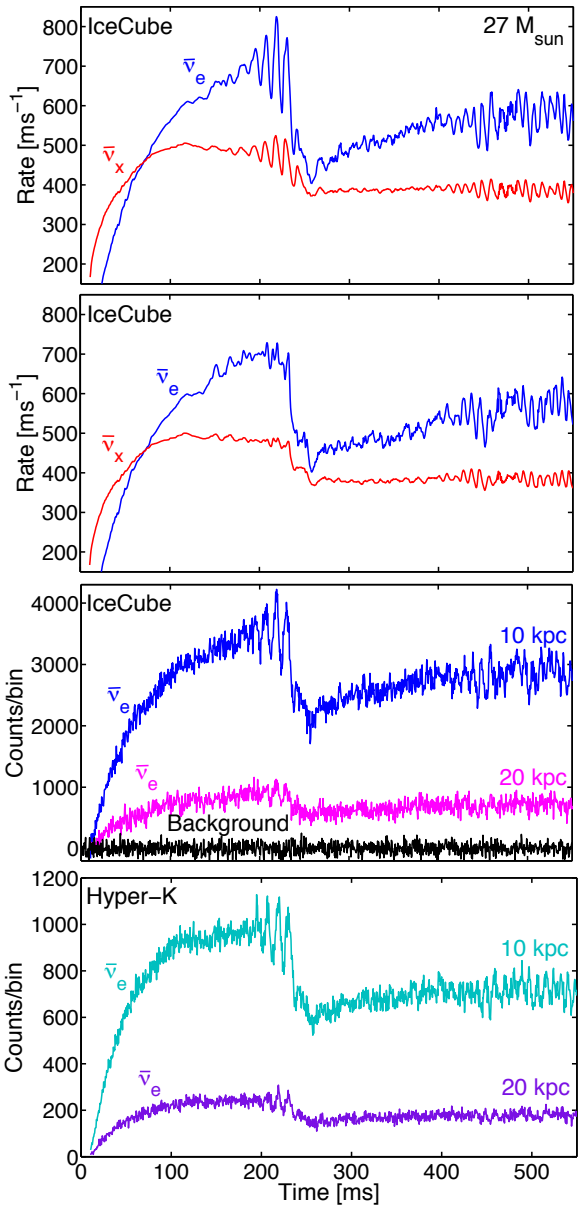

Fig. 1. Detection rate for the 27 $M_\odot$ SN progenitor, upper panels for IceCube, bottom one for Hyper-K. The observer direction is chosen for strong signal modulation, except for the second panel (minimal modulation). Upper two panels: IceCube rate at 10 kpc for $\bar{\nu}_e$ (no flavor conversion) and for $\bar{\nu}_x$ (complete flavor conversion). The lower two panels include a random shot-noise realization, 5 ms bins, for the indicated SN distances. For IceCube also the background fluctuations without a SN signal are shown.

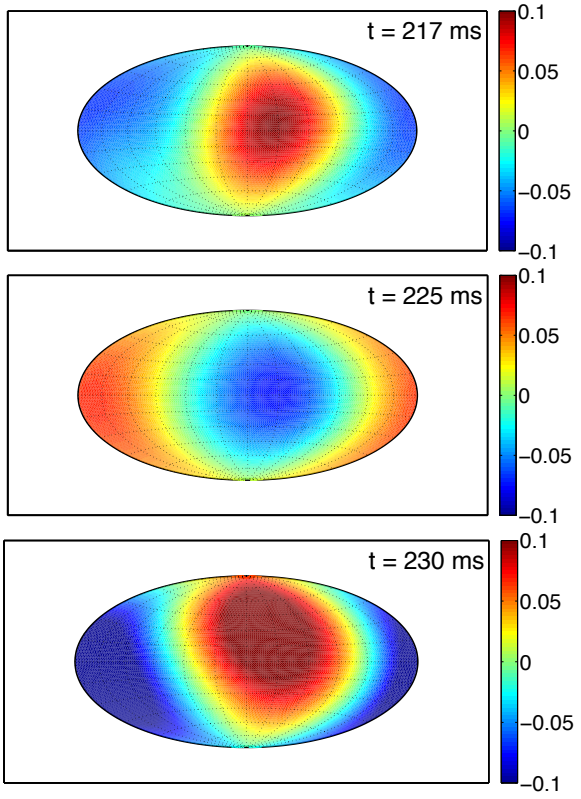

Fig. 2. IceCube detection rate for our 27 $M_\odot$ SN progenitor on a 4π map for $t = 217, 225, 230$ ms.

In the third panel of Fig. 1 we show the IceCube $\bar{\nu}_e$ signal in 5 ms bins, including a random shot noise realization since the main limitation to observing signal modulations are random fluctuations in the detected neutrino time sequence. The SASI modulation of the neutrino signal will be clearly visible for a SN up to 20 kpc (roughly the edge of the expected galactic SN distance distribution [28]).

In the bottom panel of Fig. 1, we show the expected signal in Hyper-K. For SN distances beyond some 10 kpc, the future Hyper-K detector would be superior to IceCube. In fact in spite of its smaller signal rate (about 1/3 of IceCube), its lack of background implies a better signal-to-noise ratio because of reduced shot noise for those distances where IceCube is dominated by background fluctuations. To exploit the full Hyper-K potential, its event-by-event energy determination should be used as well.

The observed signal is strictly dependent on the location of the observer and, for fixed location of the observer, the detected rate oscillates with time. We show in Fig. 2 three snapshots of the detection rate at the observer for $t = 217, 225, 230$ ms. Note as, due to the modulation of the emitted neutrino signal, locations with the highest detection rate became afterwords the ones with lowest rate and viceversa.

As a static visualization we show in Fig. 3 the relative amplitude of the IceCube detection rate during the first SASI episode. To define this amplitude we first note that the signal rate, averaged over all directions is not modulated. In a given direction we define the relative time-dependent rate and consider its root mean square deviation for the first SASI episode ($[t_1, t_2] = [120, 250]$ ms),

$$\sigma \equiv \left(\int_{t_1}^{t_2} dt \left[\frac{R - \langle R \rangle}{\langle R \rangle} \right]^2 \right)^{1/2} . \tag{1}$$

The time integrated analysis still reveals a dominant sloshing direction, which is responsible for two signal "hot spots" in two opposite directions, surrounded by directions with much smaller modulations. We can

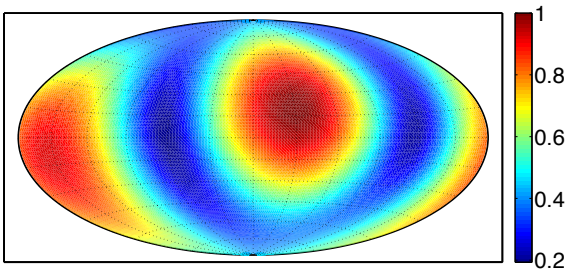

Fig. 3. Relative amplitude of the $\bar{\nu}_e$ rate modulation (see Eq. 1) on a sky-plot of observer directions during the first SASI episode (120–250 ms) of the 27 $M_\odot$ model.

conclude that almost the 50% of the locations an observer will be able to detect SASI.

4. Detection perspectives: Other progenitors

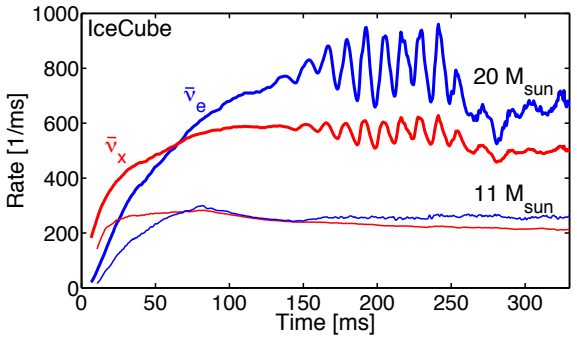

Fig. 4. IceCube rate for optimal observing directions for the 11.2 and 20 $M_\odot$ models at 10 kpc, as in the top panel of Fig. 1.

Figure 4 shows the IceCube rate for the other two analyzed progenitors (11.2 and 20 $M_\odot$) in optimal observing directions. For the heavier case, a strong SASI phase appears for $t \in [140, 300]$ ms. For this progenitor, the signal large-amplitude modulations are more pronounced than for the 27 $M_\odot$ progenitor, only one SASI phase occurs. Moreover, the SASI plane is different from the one of the 27 $M_\odot$ SN progenitor and this is clearly shown in Fig. 5 where, analogously to Fig. 3, we plot the relative amplitude of the $\bar{\nu}_e$ rate modulation (as in Eq. 1) on a sky-plot of observer directions during the SASI episode.

The 11.2 $M_\odot$ model exhibits neutrino-driven convection without any clear signs of large-amplitude coherent SASI motions (see Fig. 4). The detection rate for this progenitor is smaller than for the other two progenitors because of a lower luminosity.

Following Ref. [13], we illustrate the signal for the three progenitors in terms of its Fourier power spectrum for $t \in [100, 300]$ ms (where SASI develops for our progenitors). With the adopted signal duration of $\tau = 200$ ms, the spacing of the discrete Fourier frequencies is $\delta f = 1/\tau = 5$ Hz. Where we use the IceCube dark current as a natural baseline and adopt its power to normalize the signal power spectrum.

Figure 6 shows the power spectrum of the IceCube event rate for our three SN models thus normalized. A clear peak exists at ~80 Hz for the 27 and 20 $M_\odot$ progenitors where strong SASI appears. Note that for both the two heavier progenitors the SASI frequencies are similar because of similar neutron star radii (the same equation of state is used) and mean shock radii in the first 250 ms after bounce.

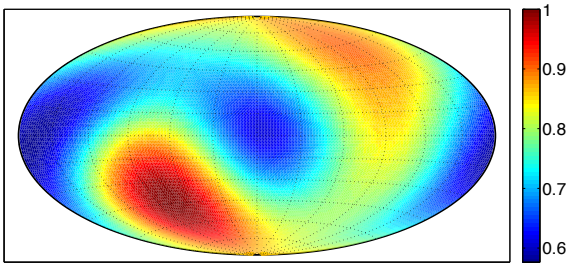

Fig. 5. Relative amplitude of the $\bar{\nu}_e$ rate modulation (see Eq. 1) on a sky-plot of observer directions during the SASI episode (140–300 ms) of the 20 $M_\odot$ model.

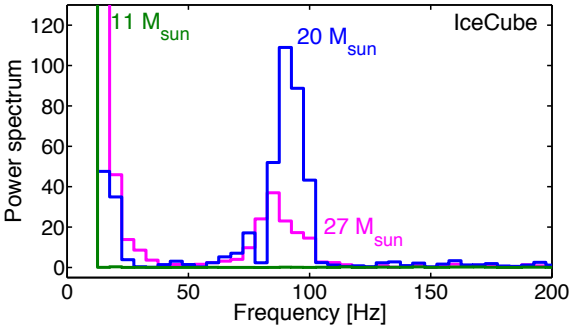

Fig. 6. Power spectrum of the IceCube event rate on the interval 100–300 ms for our three progenitors, assuming the $\bar{\nu}_e$ signal from a distance of 10 kpc. Normalization is to the frequency-independent power of shot noise caused by the IceCube background of 1.48×10^3 ms^{-1}.

5. Conclusions

The first 3D SN simulations with sophisticated neutrino transport are available for 11, 20 and 27 $M_\odot$ SN progenitors. They show pronounced spiral SASI activity for the two more massive progenitors, while the lighter one is dominated by large-scale convective overturn activity.

Such detectable instabilities appear to be dependend on the progenitor properties. If detected by IceCube and the future Hyper-K, the neutrino signal of the next galactic SN will offer a unique opportunity to diagnose different types of hydrodynamical instabilities and to test the supernova explosion mechanism.

6. Acknowledgments

The results presented here were obtained in Refs. [27, 29]. The authors are grateful to the TAUP 2013 organizers for kind hospitality.

References

[1] H. A. Bethe and J. R. Wilson, Astrophys. J. **295**, 14 (1985).
[2] H.-T. Janka, Ann. Rev. Nucl. Part. Sci. **62**, 407 (2012).
[3] H. A. Bethe, Rev. Mod. Phys. **62**, 801 (1990).
[4] J. M. Blondin, A. Mezzacappa and C. DeMarino, Astrophys. J. **584**, 971 (2003).
[5] L. Scheck, H.-T. Janka, T. Foglizzo and K. Kifonidis, Astron. Astrophys. **477**, 931 (2008).
[6] J. M. Blondin and A. Mezzacappa, Nature (London) **445**, 58 (2007).
[7] W. Iwakami *et al.*, Astrophys. J. **700**, 232 (2009).
[8] R. Fernández, Astrophys. J. **725**, 1563 (2010).
[9] T. Foglizzo, F. Masset, J. Guilet and G. Durand, Phys. Rev. Lett. **108**, 051103 (2012).

[10] F. Hanke *et al.*, Astrophys. J. **770**, 66 (2013).
[11] J. W. Murphy, C. D. Ott and A. Burrows, Astrophys. J. **707**, 1173 (2009).
[12] B. Müller, H.-T. Janka and A. Marek, Astrophys. J. **766**, 43 (2013).
[13] T. Lund *et al.*, Phys. Rev. D **82**, 063007 (2010).
[14] T. Lund *et al.*, Phys. Rev. D **86**, 105031 (2012).
[15] B. Müller, H.-T. Janka and A. Heger, Astrophys. J. **761**, 72 (2012).
[16] R. Abbasi *et al.* (IceCube Collaboration), Astron. Astrophys. **535**, A109 (2011).
[17] K. Abe *et al.* (Super-Kamiokande Collaboration), Phys. Rev. D **83**, 052010 (2011).
[18] K. Abe *et al.*, arXiv:1109.3262.
[19] S. E. Woosley, A. Heger and T. A. Weaver, Rev. Mod. Physics **74**, 1015 (2002).
[20] S. E. Woosley and A. Heger, Phys. Rep. **442**, 269 (2007).
[21] R. Buras, M. Rampp, H.-T. Janka and K. Kifonidis, Astron. Astrophys. **447**, 1049 (2006).
[22] M. Rampp and H.-T. Janka, Astron. Astrophys. **396**, 361 (2002).
[23] A. Marek *et al.*, Astron. Astrophys. **445**, 273 (2006).
[24] E. Müller, H.-T. Janka and A. Wongwathanarat, Astron. Astrophys. **537**, 63 (2012).
[25] M. T. Keil, G. G. Raffelt and H.-T. Janka, Astrophys. J. **590**, 971 (2003).
[26] I. Tamborra *et al.*, Phys. Rev. D **86**, 125031 (2012).
[27] I. Tamborra, F. Hanke, B. Müeller, H. -T. Janka and G. Raffelt, Phys. Rev. Lett. **111** (2013) 121104.
[28] S. M. Adams *et al.*, Astrophys. J. **778** (2013) 164.
[29] I. Tamborra *et al.*, in preparation.